PCCP

RSC Publishing

PAPER

View Article Online
View Journal | View Issue

Cite this: *Phys. Chem. Chem. Phys.*, 2013, **15**, 15954

Development and application of effective pairwise potentials for UO_2^{n+}, NpO_2^{n+}, PuO_2^{n+}, and AmO_2^{n+} (n = 1, 2) ions with water†

Vladimir Pomogaev,[a] Surya Prakash Tiwari,[a] Neeraj Rai,[a] George S. Goff,[b] Wolfgang Runde,[b] William F. Schneider*[c] and Edward J. Maginn*[d]

Received 13th June 2013,
Accepted 8th August 2013

DOI: 10.1039/c3cp52444b

www.rsc.org/pccp

Intra- and intermolecular force field parameters for the interaction of actinyl ions (AnO_2^{n+}, where, An = U, Np, Pu, Am and n = 1, 2) with water have been developed using quantum mechanical calculations. Water was modeled with the extended simple point charge potential (SPC/E). The resulting force field consists of a simple form in which intermolecular interactions are modeled with pairwise Lennard-Jones functions plus partial charge terms. Intramolecular bond stretching and angle bending are treated with harmonic functions. The new potentials were used to carry out extensive molecular dynamics simulations for each hydrated ion. Computed bond lengths, bond angles and coordination numbers agree well with known values and previous simulations. Hydration free energies, computed from molecular dynamics simulations as well as from quantum simulations with a solvation model, were in reasonable agreement with estimated experimental values.

1 Introduction

Understanding the behavior of actinides in aqueous solution is critical for performance assessments of geologic radioactive waste disposal and storage sites and to develop separation and partitioning processes for used nuclear fuel. The scientific challenge for the management of the continuously increasing large volumes of used nuclear fuel is to develop effective and selective methods for separating the radioelements, including in particular U, Np, Pu, and Am, from waste mixtures using ion exchange, solvent extraction, or electrodeposition. The chemistry of the light actinides is extremely rich, with multiple oxidation states stable at relevant conditions. The oxidation states ultimately determine the environmental behavior of the actinides, as well as the effectiveness and performance of separations processes. In general, actinides in their +III and +IV oxidation states are less soluble and easily adsorb on mineral and soil surfaces, while the +V and +VI oxidation states exhibit higher solubilities in aqueous solutions. In their common lower (+III and +IV) oxidation states these elements appear as simple cations, but in their higher oxidation states they form discrete actinyl ions, AnO_2^{n+}, n = 1, 2.[1] The stability of dioxo actinyl in the +V and +VI oxidation states varies significantly for U, Np, Pu, and Am.[2–5] Although generating isolated gas phase actinyl ions has been a challenge,[6] they are present in aqueous solutions coordinated with water molecules or other ligands in the equatorial plane around the actinide center, as confirmed by experimental measurements of hydration enthalpy and entropy,[6–10] oxidation state,[11,12] spectral properties,[9,13–16] and other processes and properties.[3,6,17–19,20]

The radiotoxicity of these heavy elements presents a challenge in carrying out experimental studies. Quantum and classical molecular simulations are alternative means for obtaining thermodynamic, structural, and other properties of actinide species in the condensed phase.[21] Explicitly modeling solvated actinide ions quantum mechanically, however, is difficult and computationally costly. Classical force field-based simulations of these systems are a viable alternative, but the accuracy of such simulations relies upon the ability of the force field to accurately capture intra- and intermolecular interactions. Force fields are often parametrized against experimental data, but due to the scarcity of suitable experimental data for the actinides, this is not a viable approach in the present case. An alternative approach for developing force fields is to perform quantum mechanical calculations on relatively small model systems to generate a potential energy surface (PES) for the

[a] *Department of Chemical and Biomolecular Engineering, University of Notre Dame, 182 Fitzpatrick Hall, Notre Dame, IN 46556, USA*
[b] *Los Alamos National Laboratory, Los Alamos, New Mexico 87545, USA*
[c] *Department of Chemical and Biomolecular Engineering and Department of Chemistry and Biochemistry, University of Notre Dame, 182 Fitzpatrick Hall, Notre Dame, IN 46556, USA. E-mail: wschneider@nd.edu; Fax: +1 574 631 8366; Tel: +1 574 631 8754*
[d] *Department of Chemical and Biomolecular Engineering, University of Notre Dame, 182 Fitzpatrick Hall, Notre Dame, IN 46556, USA. E-mail: ed@nd.edu; Fax: +1 574 631 8366; Tel: +1 574 631 5687*

† Electronic supplementary information (ESI) available. See DOI: 10.1039/c3cp52444b

species of interest and then fit the PES to an analytic potential function. Once the force field is in hand, condensed phase molecular dynamics (MD) and Monte Carlo (MC) simulations can be performed to determine thermodynamic, structural and dynamical properties of bulk systems. Here, we are interested in developing potentials for the AnO_2^{n+}, n = 1, 2 ions with a common model for water, the non-polarizable extended simple point charge (SPC/E) model.[22] SPC/E is a commonly used water model that has been shown to give accurate structural, thermodynamic and transport properties.[23] Other water models could be used following the procedures outlined here.

Our previous work[24] on the aqueous uranyl(VI) ion demonstrated the importance of using an explicitly "solvated" UO_2^{2+} complex when computing the water–uranyl PES, as opposed to a single water molecule. Similar methods had been applied to other high oxidation state actinide ions and in developing potentials for interacting ionic species[25–27] when electron transfer from one monomer (anion) to the other (cation) makes it impossible to generate a PES for correct electronic states. In the condensed phase these ions are stabilized by solvation effects and do not exhibit the extensive charge transfer found for an unsolvated "bare" ion in the gas phase. To suppress the electron transfer, one can use extra water molecules to explicitly solvate the ionic species while generating potential energy surfaces.[24–28] Such an approach mimics many-body solvation effects that prevent electron transfer between an actinyl cation and water molecules and has been tested for four popular water models including SPC/Fw,[23] TIP3P,[29] TIP4P,[29] and TIP5P.[30]

Following our earlier work,[24] here we develop intra- and intermolecular force fields for AnO_2^{n+} (An = U, Np, Pu, Am; n = 1, 2) in water. Little information on intramolecular parameters for the deformation of O═An═O bonds and angles are available in the literature.[31–33] In an earlier study[24] on UO_2^{2+}, the force constants for harmonic bond stretching and angle bending terms were taken from the work of Guilbaud and Wipff.[31] In the present study, these intramolecular force constants are obtained for all the actinyl ions by fitting *ab initio* PESs to harmonic functional forms. Non-bonded Lennard-Jones parameters and partial charges for AnO_2^{n+} ions in the SPC/E model of water are determined and used to compute structural, thermodynamic and dynamic properties of the ions in water. The impact of the new intramolecular potential parameters on condensed phase properties is tested by carrying out additional simulations of UO_2^{2+} with SPC/Fw, TIP3P, TIP4P, and TIP5P water models, using intermolecular parameters developed in our previous work[24] but the new intramolecular parameters obtained in the present study.

2 Computational methods

2.1 Quantum mechanical calculations

All electronic structure calculations were performed with the Gaussian 09 program suite.[34] We employed quantum chemical methods consistent with those described and validated in the previous work on UO_2^{2+}. Scalar relativistic effects were included by means of Stuttgart relativistic energy-consistent small-core pseudopotentials, which include one-component relativistic effective-core potentials (RECP60MWB).[35] The corresponding ECP60MWB-ANO atomic natural orbital (ANO) valence basis sets for the actinides were used.[36,37] Intra- and intermolecular potentials were calculated using an augmented correlation-consistent polarized valence triple zeta (aug-cc-pVTZ)[38] and augmented polarized weighted core/valence triple zeta (aug-cc-pwCVTZ)[39] basis sets were employed for the hydrogen and oxygen atoms, respectively. The aug-cc-pwCVTZ basis set in the Gaussian format was downloaded from the EMSL basis set exchange database[40,41] while ECP60MWB-ANO basis in the Gaussian format was downloaded from the Stuttgart/Köln group basis set library.[42]

Intramolecular potentials were calculated using the B3LYP hybrid density functional.[43–45] Intermolecular potentials are more sensitive to dispersion interactions and were derived at the MP2 level[46] using an $AnO_2^{n+}(H_2O)_4$ model and implicit solvation corrections. Initial structures were optimized in D_{4h} symmetry and then used for generating PESs between three-coordinated actinyl species and a fourth water molecule. Implicit solvation calculations used the polarizable continuum model implemented with the integral equation formalism (IEF-PCM).[47] PCM calculations used the universal force field radii as implemented default in the Gaussian code, a water dielectric constant ε = 78.355300 and ε^{∞} = 1.777849, and van der Waals radii scaled by 1.100. All other internal degrees of freedom were fixed during these potential energy scans. The counterpoise method of Boys and Bernardi[48] was employed to correct for basis set superposition error (BSSE).[24,48]

The non-bonded interactions were modeled with pairwise Lennard-Jones (LJ) and Coulomb potentials while bond stretching and angle bending were modeled with harmonic functions, yielding a traditional "class I" type force field. The total energy of the system is given by

$$U_{\text{total}} = \sum_{i,j}\left[4\varepsilon_{ij}\left(\left(\frac{\sigma_{ij}}{r_{ij}}\right)^{12}-\left(\frac{\sigma_{ij}}{r_{ij}}\right)^{6}\right)+\frac{q_i q_j}{4\pi\varepsilon_0 r_{ij}}\right] + \sum_{i=1}^{n\text{bonds}}\frac{1}{2}k_l(l_i-l_0)^2+\sum_{i=1}^{n\text{angles}}\frac{1}{2}k_\theta(\theta_i-\theta_0)^2 \quad (1)$$

where the first summation is over all intermolecular atom pairs i,j, the second summation is over all flexible bonds l_i, and the third summation is over all flexible angles θ_i. The terms r_{ij}, σ_{ij}, ε_{ij}, q_i, q_j, and ε_0 are the separation between two interacting sites, LJ size, LJ well depth, partial atomic charge on sites i and j, and the permittivity of vacuum, respectively. The force constants k_l and k_θ govern bond stretching about the nominal bond length l_0 and angle bending about the nominal bond angle θ_0, respectively. Note that nonbonded interactions are only computed between sites on different ions/molecules.

Hydration free energies were estimated in the hybrid explicit/implicit "discrete supermolecular-continuum" model successfully applied in other quantum chemical studies.[49–59] The DFT-B3LYP level of theory and IEF-PCM were used based on the good performance found for similar calculations performed on the

hydration of dipositive and monopositive actinyl and hydroxoactinyl ions.[52,56–67] Both prior experiment and present molecular dynamics suggest five H_2O in the first hydration shell; we use five asymmetric equatorial H_2O in these hybrid solvation calculations for all cations. For computational expediency in these C_1 calculations, more modest 6-31G(d) and 6-21G basis sets were used for oxygen and hydrogen, respectively. Intramolecular contributions to the free energies were estimated using the ideal gas/harmonic oscillator approximation at T = 298.15 K. The hydration free energy ΔG°_{hyd} is approximated as the difference in free energy between a final hydrated product, the gas-phase ion, and solvated water molecules:[55]

$$AnO_2^{n+}(g) + 5H_2O(aq) \rightleftharpoons [AnO_2(H_2O)5]^{n+}(aq)$$

$$\Delta G^{\circ}_{hyd}(AnO_2^{n+}) = \tilde{G}^{\circ}\left(\left[AnO_2(H_2O)_5\right]^{n+}\right) - G^{\circ}(AnO_2^{n+}) - 5\tilde{G}^{\circ}(H_2O) \quad (2)$$

where G° and $\tilde{G}^{\circ}$ are the free energies of gas-phase and PCM-solvated species, respectively. The water free energy was calculated at an effective pressure of 1354 atm corresponding to a 55.5 molar density and solvated ions at 24.4 atm corresponding to 1 M.[52,57,58,61,62,68]

2.2 Classical simulations

GROMACS-4.5.5[69,70] with single precision was used for all MD simulations. The simulation system consisted of one actinyl ion and 1000 water molecules in cubic box of approximately 3.12 nm length. Periodic boundary conditions were applied in all three directions. A modified switch type particle mesh-Ewald (PME) method[71,72] was used to handle long range electrostatic interactions. A uniform background charge was used to neutralize the system. Both LJ interactions and real space PME interactions were smoothly switched off to zero at 1.2 nm with the switching starting at 1.1 nm. A Fourier grid spacing of 0.12 nm was used for the PME in reciprocal space. After an initial steepest descent energy minimization, 100 ps of canonical ensemble (NVT) simulations at 298.15 K, and then 200 ps of isothermal–isobaric ensemble (NPT) simulations at 1 bar and 298.15 K were carried out for equilibration. A time step of 0.002 ps was used for all the rigid water models (SPC/E, TIP3P, TIP4P, TIP5P), while 0.0005 ps was used for simulations with the flexible SPC/Fw water model. Bonds of rigid water molecules were constrained using SETTLE.[73]

For calculations of properties other than hydration free energy, a leap-frog algorithm was used for integrating the equations of motion. Production runs of 150 ns were performed in the NVT ensemble at 298.15 K using a weak Nosé–Hoover thermostat[74] with a time constant of 6 ps. Average pressure close to 1 bar was obtained by choosing the box lengths averaged from a previously equilibrated NPT ensemble simulation of 4 ns at 1 bar and 298.15 K. The initial 5 ns of data from the NVT production run were discarded as equilibration.

For hydration free energy calculations, a leap-frog stochastic dynamics (SD) integrator was used for integrating the equations of motion. NPT ensemble simulations at 1 bar (Parrinello-Rahman barostat with time constant of 2 ps) and 298.15 K (stochastic temperature-coupling with time constant of 2 ps) were run for 2 ns after initial equilibration for each point (Hamiltonian perturbed). Bennett's acceptance ratio (BAR) method[75] was used to calculate the change in free energies. Additional details on the methodology to calculate hydration free energies and corrections terms may be found in our previous work.[24] Example input files are provided in ESI.†

Radial distribution functions, coordination numbers, and hydration free energies were calculated for all eight actinyl ions in SPC/E water. Additional studies were performed on UO_2^{2+} in water modeled with the SPC/Fw, TIP3P, TIP4P, and TIP5P potentials. For these calculations, the interactions between UO_2^{2+} and water were taken from Rai *et al.*[24] but the newly developed intramolecular parameters were used for the uranyl ion to test the impact this has on properties. Analysis programs available in the Gromacs 4.5.5 suite were used to calculate all these properties.

3 Results and discussions

3.1 Intramolecular potential parameter development

To obtain parameters for the harmonic bond stretching and angle bending terms in eqn (1), the structures of each actinyl ion were optimized in the gas phase at the B3LYP level of theory. Geometry results for the isolated actinyls are summarized in Table 1. The An═O actinyl bond lengths decrease slightly across the series (U, Np, Pu, Am) and are slightly longer for the mono- than dications. Intramolecular PESs were derived by perturbing the bond distances in 0.0005 nm increments up to a maximum displacement of 0.005 nm and separately bond angles in 0.1° increments up to 1.0° maximum. For all the ions, the perturbed energies were closely harmonic and easily fit the harmonic functional forms in eqn (1) to yield intramolecular force constants (k_l and k_θ). In general, stretching modes become softer and bending modes stiffer across the series. The UO_2^{2+} force constants derived here are significantly softer than literature values used in other force fields.[31]

The bond lengths l_0' obtained in this manner yield potentials that, when used in MD simulations, underpredict experimentally observed bond lengths. An═O distances are sensitive to water

Table 1 Bond length of isolated AnO_2^{n+} and intramolecular force field parameters and partial atomic charges for AnO_2^{n+}. The bond lengths used in the classical potentials are in bold font

AnO_2^{n+}	$l_0'^a$	l_0^b	k_l^c	k_0^d	q_{An}(e)	q_{OAn}(e)
UO_2^{2+}	0.169	**0.176**	622 300	198	2.50	−0.25
NpO_2^{2+}	0.169	**0.173**	595 900	236	2.52	−0.26
PuO_2^{2+}	0.166	**0.170**	595 900	602	2.47	−0.235
AmO_2^{2+}	0.165	**0.168**	598 100	791	2.50	−0.25
UO_2^{+}	0.174	**0.181**	514 700	224	2.08	−0.54
NpO_2^{+}	0.172	**0.178**	516 700	395	2.08	−0.54
PuO_2^{+}	0.170	**0.174**	527 600	563	2.04	−0.52
AmO_2^{+}	0.171	**0.172**	477 300	533	1.80	−0.40

[a] Isolated An═O bond lengths in nm. [b] Solvated An═O bond lengths in nm from $AnO_2^{n+}(H_2O)_4$. [c] Units are (kJ mol^{-1} nm^{-2}). [d] Units are (kJ mol^{-1} rad^{-2}).

coordination. We reoptimized the AnO_2^{n+} ions with a first solvation shell of four water molecules, in D_{4h} symmetry with PCM. The "solvated" bond lengths l_0 are shown in Table 1 in bold type. The addition of ligating water and the use of a continuum solvation field produce a positive shift in these bond distances of 0.001 to 0.007 nm. The An–OH_2 distances are approximately 0.06 nm greater than the An=O distances and follow essentially the same periodic trends. Since the solvated bond lengths are in better agreement with experimental data,[5,13,52,67,76–86] they were used while fitting to get intermolecular potential parameters, and also in subsequent MD simulations.

3.2 Intermolecular potential parameter development

Water molecules associate strongly with all the actinyl ions, binding through the water oxygen in the actinyl equatorial plane. As more water molecules are added to the equatorial plane, the differential interaction energy between any given water molecule and the ion decreases. For example, we compute the binding energy of H_2O to $[UO_2(H_2O)]^{2+}$ to be 15% less than the binding energy to UO_2^{2+}. The binding energy per water molecule is 30% less in $[UO_2(H_2O)_4]^{2+}$ than it is in $[UO_2(H_2O)]^{2+}$.[24] Similar results are found for the other actinyls. The interaction potential between H_2O and the actinyls is clearly sensitive to the number of water molecules in the first coordination sphere. In keeping with our previous procedures, then, actinyl–water potential energy surfaces were computed starting from D_{4h} $[AnO_2(H_2O)_4]^{n+}$ structure and repositioning and perturbing the location of one of the water molecules along three different displacement paths, as shown in Fig. 1. In configuration P, r_0 is the distance between An and O of water obtained by optimizing $[AnO_2(H_2O)_4]^{n+}$. The same distance (r_0) is used between An and O of frozen waters in all the configurations. As the two other configurations considered in the previous work[24] were largely repulsive and did not affect the final force field parameters, they were not included in the present work. For the purposes of developing potentials, electronic configurations of ground states were identified for isolated units and preserved for the same species in all calculations with water as coordinated actinyl ligands. This preservation is possible due to the weak ligand field.[52]

Non-bonded force field parameters (σ_{ij}, ε_{ij}, q_i, q_j) were developed in a manner similar to our previous work,[24] with minor differences. Starting from the D_{4h} structures, one of the equatorial waters was (re)positioned in the equatorial (E), T-shaped (T), or parallel (P) location, displaced along the paths illustrated in Fig. 1, and interaction energies computed as:

$$U_{Int} = \{E[[AnO_2(H_2O)_3]^{n+} + H_2O] - E[[AnO_2(H_2O)_3]^{n+}]\} - \{E[(H_2O)_3 + H_2O] - E[(H_2O)_3]\} \quad (3)$$

where U_{Int} and E[X] represent interaction energy and the electronic energy of species X computed in supermolecular basis, respectively. The results of these potential energy scans are shown in Fig. 2, referenced to the infinite separation limit. All PESs show similar qualitative features, with the 1+ ion surfaces shifted upward approximately 80 kJ mol^{-1} relative to the 2+. To obtain the intermolecular potential parameters in eqn (1) for each ion, the mean squared difference between the MP2 energies and the energies obtained from the potential energy function were minimized for AnO_2^{n+}–(OH_2) distances between 0.22 and 0.70 nm for the three different paths (E, T and P). SPC/E water partial charges were used. Fits were relatively insensitive to the Lennard-Jones parameters but were more sensitive to the values of the partial charges on the actinyl ion. For this reason and to keep the number of parameters to a minimum, the same Lennard-Jones parameters were assigned to each actinyl ion, but different partial charges were used. The recommended Lennard-Jones parameters are given in Table 2 while the partial charges are listed in Table 1. The charges on the actinide atom center and the apical oxygen atoms are close to +2.5 and −0.25, respectively, for all the 2+ ions. These values decrease to approximately +2 and −0.5 for the monocations.

Choppin *et al.*[87,88] estimated the effective charges on An(V) to be 2.2 and on An(VI) to range from 2.9 to 3.2 from the measured stability constants of $[AnO_2F]^{m+}$ (m = 1,0)[88] and an extended Born equation.[88] These charges are only slightly larger than the charges derived in the present work, consistent with the fact

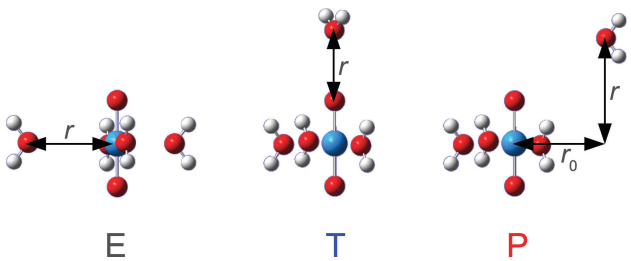

Fig. 1 E, T and P displacement coordinates for AnO_2^{n+}–water potential energy surfaces.

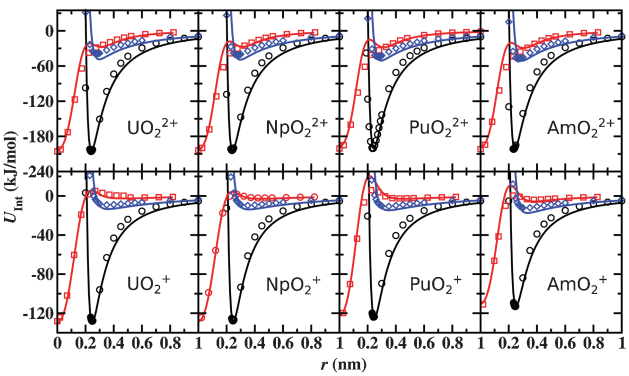

Fig. 2 AnO_2^{n+}–water potential energy scans. Black, blue and red represent E, T and P coordinates, respectively. Symbols are MP2 results and lines are fits to the LJ + Coulomb functional form using SPC/E water.

Table 2 AnO_2^{n+} – SPC/E water Lennard-Jones interaction parameters. Atom centers shown in bold type

Type	σ (nm)	ε (kJ mol^{-1})
An–Ow	0.306	0.587
OAn–**O**w	0.350	0.192

that the Born model ignores the van der Waals attraction between AnO_2^{n+} and F^- and thus tends to overestimate Coulombic interactions.

3.3 An=O_{An} and An···O_w lengths

MD simulations were carried out in SPC/E water using the derived force field parameters. The simulations show that all the cations prefer to be five-fold coordinated in bulk water (*vide infra*). Computed An=O_{An} and An···O_w bond lengths are in good agreement with both experiment[5,13,52,67,76–82] and previous computational studies,[12,56–58,67,89] as shown in Table 3.

The structure of the mono- and dications in a field of five equatorial water were also calculated using the B3LYP model and PCM solvation. Calculations in five-fold D_{5h} symmetry generally produced several imaginary vibrational modes. Breaking the symmetry and relaxing resulted in the C_1 structures illustrated in Fig. 3, similar to those reported previously.[56] Bond distances and angles are similar to the high symmetry results, but internal dihedrals differ. The lower symmetry structures have all real vibrational modes. The D_{5h} and C_1 structural parameters are summarized in Table 3.

As shown, they agree well with experiment[5] and previous calculations.[89] The presence of coordinating H_2O lengthens the An=O bonds compared to the free cations, and again lengths decrease slightly across the series and are slightly longer for the mono- than dications. Similar trends are observed for the An–OH_2 distances.

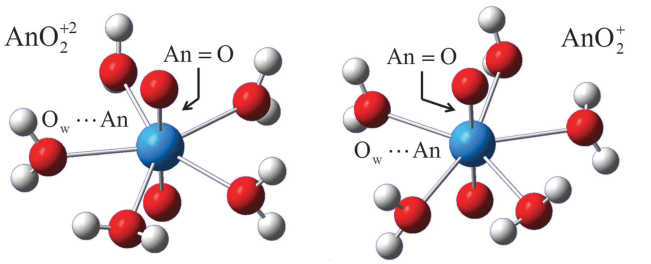

Fig. 3 Typical pentaaquo structures.

3.4 Radial distribution functions

Radial distribution function (RDF) and number integral (NI) plots for each actinyl ion's actinide atom with the oxygen atom of SPC/E water (An···O_w) and actinyl ion's oxygen atom with hydrogen atom of SPC/E water (O_{An}···H_w) are shown in Fig. 4. Computed coordination numbers are compared with literature values in Table 4. The NIs for An···O_w show that all the cations prefer to be coordinated by five water molecules in the first solvation shell, with the exception of AmO_2^+, where the computed value was 4.86. As expected, the RDF and NI plots of both An···O_w and O_{An}···H_w for the dication actinyls heavily overlap each other,

Table 3 Comparison of An=O bond lengths and An···O_w distances obtained from MD simulations and B3LYP optimizations of $AnO_2^{n+}(OH_2)_5$ ions with literature computational and experimental data

	Distance (nm)							
	UO_2^{2+}		NpO_2^{2+}		PuO_2^{2+}		AmO_2^{2+}	
	An=O	An···O_w	An=O	An···O_w	An=O	An···O_w	An=O	An···O_w
MD[a]	0.178	0.246	0.174	0.246	0.172	0.246	0.169	0.246
B3LYP (D_{5h})	0.175	0.247	0.173	0.245	0.171	0.243	0.169	0.242
B3LYP (C_1)[b]	0.176	0.247	0.174	0.245	0.172	0.244	0.172	0.245
Experiment	0.177[76,77]	0.241[76,78,79]	0.175[80]	0.242[80]	0.174[81,82]	0.245[81]	0.191[13]	—
	0.176[78]	0.242[77]	0.190[13]		0.190[13]	0.241[82]		
	0.178[79]							
	0.190[13]							
Computation	0.176[12]	0.244[12]	0.173[12]	0.242[12]	0.171[12]	0.241[12]	0.171[12]	0.243[12]
	0.178[56,57]	0.247[57]	0.176[57]	0.246[57]	0.175[57]	0.245[57]		
		0.246[56]			0.172[56]	0.243[56]		
	Distance (nm)							
	UO_2^+		NpO_2^+		PuO_2^+		AmO_2^+	
	An=O	An···O_w	An=O	An···O_w	An=O	An···O_w	An=O	An···O_w
MD[a]	0.183	0.254	0.180	0.254	0.177	0.256	0.174	0.258
B3LYP (D_{5h})	0.182	0.256	0.179	0.255	0.176	0.253	0.175	0.255
B3LYP (C_1)[b]	0.183	0.258	0.180	0.256	0.179	0.257	0.179	0.258
Experiment	—	—	0.183[67,78]	0.250[67,78]	0.181[13,82]	0.247[67,78,82,83]	0.195[13]	—
			0.182[80]	0.249[80,84]	0.184[81]	0.245[81]		
			0.196[13]	0.251[83]				
				0.252[85,86]				
Computation	0.181[12]	0.251[12]	0.177[12]	0.249[12]	0.174[12]	0.249[12]	0.171[12]	0.251[12]
	0.182[57]	0.257[57]	0.181[56,57]	0.257[57]	0.180[57]	0.257[57]		
	0.180[67]	0.260[67]	0.179[67]	0.260[67]	0.177[67]	0.260[67]		
				0.252[56]				

[a] Statistical uncertainty in An=O lengths is 0.002 nm. An···O_w lengths were obtained from the first maximum in the An···O_w radial distribution function. [b] Average An···O_w distances reported.

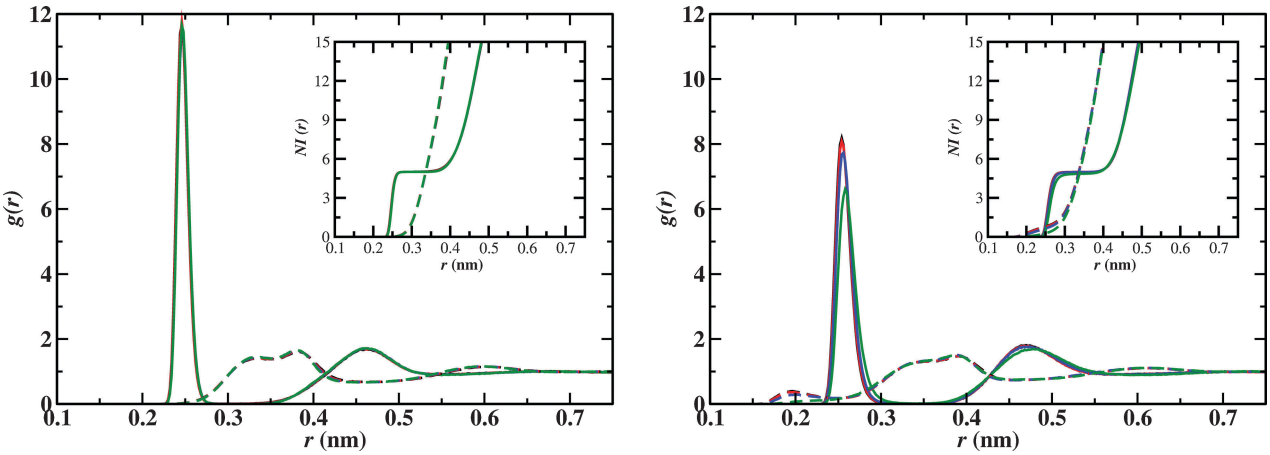

Fig. 4 RDFs and number integrals (inset) of An···O_w (solid lines) and O_{An}···H_w (broken lines) for (a) AnO_2^{2+} and (b) AnO_2^{+} in SPC/E water. Black, red, blue and green lines represent RDFs for U, Np, Pu and Am, respectively. Overlap obscures the colors in some places.

Table 4 Coordination number (N) in the first solvation shell of AnO_2^{n+} in SPC/E water compared with available literature results

AnO_2^{n+}	N_{MD}[a]	$N_{Computational}$[b]	$N_{Theoretical}$[c]	$N_{Experimental}$[c,d]
UO_2^{2+}	5.0067_3	$5^{32,49,52,66,90}$	5.2	4.5, 5, 6
NpO_2^{2+}	5.0019_1	$5^{52,66}$	5.3	5, 6
PuO_2^{2+}	5^e	$5^{49,52,66}$	5.5	5, 6
AmO_2^{2+}	4.9999^e	5^{12}	5.9	—
UO_2^{+}	4.9913_5	$5^{52,66}$	4.5	5
NpO_2^{+}	4.9895_6	$5^{52,66}$	3.9	4, 5, 6
PuO_2^{+}	4.9799_7	$5^{52,66}$	3.6	3.3, 4, 5
AmO_2^{+}	4.8550_{20}	5^{12}	3.8	—

[a] From this work, using MD simulations. [b] Computational studies other than this work. [c] Taken from the work of Mauerhofer *et al.*[91] and citations therein. [d] Taken from the works of Antonio *et al.*,[92] Knope *et al.*[5] and citations therein. [e] Uncertainty is less than 0.0001.

Table 5 Computed and inferred hydration free energies (ΔG_{hyd}) in kJ mol^{-1} at T = 298.15 K

AnO_2^{n+}	MD[a]	DFT[b]	DFT[c]	exp't[d]	$\Delta H_{hyd}^{exp't}$	$T\Delta S_{hyd}^{exp't}$
UO_2^{2+}	−1390	−1702	−1730	−1546	−1665	−119
NpO_2^{2+}	−1389	−1703	−1726	−1565	−1687	−122
PuO_2^{2+}	−1372	−1697	−1713	−1549	−1671	−122
AmO_2^{2+}	−1376	−1644		>−1774	>−1896	−122
UO_2^{+}	−499	−716	−716	−613	−709	−96
NpO_2^{+}	−492	−709	−735	−658	−754	−96
PuO_2^{+}	−474	−670	−704	−649	−746	−97
AmO_2^{+}	−417	−639		−682	−776	−94

[a] Statistical uncertainty in ΔG_{hyd} from MD are less than 1 kJ mol^{-1}. [b] This work. [c] Ref. 57 and 58. [d] Inferred from observed/estimated enthalpies[6] and entropies.[8]

whereas some differences can be seen in the RDF plots for monocation actinyls, especially for AmO_2^{+} which has a relatively weak association with water compared to other monocations. This is due to the fact that the charge on Am is 1.8 compared to approximately 2 for the other monocations. Peak positions of the first maximum in each RDF of An···O_w are given in Table 3, and are also compared with available literature values. RDFs of O_{An}···H_w for monocations have a small peak at around 0.2 nm which is absent in RDFs for dications. This small peak suggests that the higher charged O for monocations, compared to that for dications, attracts the hydrogen atom of water more readily near axial regions of actinyl ion. The small peak is not prominent in the RDF for AmO_2^{+}, whose oxygen atom has a smaller charge (−0.4) compared to approximately −0.5 for other monocations.

3.5 Hydration free energies (ΔG_{hyd})

ΔG_{hyd} from MD simulations, quantum calculations (DFT), and estimated from experiments are summarized in Table 5 for all the actinyl ions studied in this work. ΔG_{hyd} of AnO_2^{2+} ions from the MD and quantum approaches are close to −1380 kJ mol^{-1} and −1500 kJ mol^{-1}, respectively; free energies for the AnO_2^{+} ions are approximately 900–1000 kJ mol^{-1} less exothermic relative to AnO_2^{2+}. Differences of this order between dications and monocations are consistent with known experiments.

DFT-computed hydration free energies are 200 and 300 kJ mol^{-1} more exothermic for the mono- and dications, respectively. Shamov and Schreckenbach[57,58] used a similar hybrid explicit-implicit method to estimate hydration free energies of the mono- and dications of uranyl through plutonyl at the B3LYP level. Results are quite similar to those reported here, the small differences arising from detailed differences in structure and exact solvation model.

Experimental values for the hydration free energies are not available, but estimates of the hydration enthalpies[6] and entropies[8] have been reported. The entropies are in a range between −409 and −410 J mol^{-1} K^{-1} for dications and −314 and −324 J mol^{-1} K^{-1} for monocations; these values are presented in Table 5 as $T\Delta S$ at T = 298.15 K. Only a lower bound is available for the AmO_2^{2+} enthalpy and the tabulated value here reflects that lower bound. Enthalpies and entropies are combined to estimate the experimental hydration free energies at 298.15 K. The estimated errors on the experimental hydration free energies propagated from the enthalpies are of the order 50–100 kJ mol^{-1}.

As explained in our previous work[24] on UO_2^{2+}, experimental $\Delta G_{hyd}[UO_2^{2+}]$ can be bounded between −1360 ± 24 (ref. 7) to

-1665 ± 65 kJ mol^{-1}.[6] Experimental results in Table 5 are only shown from Gibson *et al.*,[6] since enthalpies for other actinyl ions are not available in the work of Marcus.[7] However, a bound similar to that of UO_2^{2+} can be formed for comparing the hydration free energy results. Results from MD simulations lie well within these bounds, though closer to the upper bound. The implicit-explicit DFT calculations are close to the lower bound.

3.6 Effect of intramolecular potential on properties

In an earlier study,[24] classical pairwise potentials were developed for UO_2^{2+} with four different models of water (SPC/Fw, TIP3P, TIP4P, and TIP5P). The intramolecular stretching and angle bending potential parameters suggested by Guilbaud and Wipff[31] were used, but these differ significantly from those determined in the present study. To assess the importance of the intramolecular potential on properties, calculations were performed for UO_2^{2+} interacting with water using intermolecular LJ parameters from the earlier work[24] but intramolecular parameters from the present study. We will refer to this as the "hybrid" UO_2^{2+} model.

RDF and NI plots between U and the oxygen on water (U$\cdots$O$_w$) are shown in Fig. 5 for the hybrid UO_2^{2+} model in different water models. The distribution functions show subtle differences from what was obtained with the same intermolecular potentials but stiffer intramolecular potentials.[24] With the original model, UO_2^{2+} was coordinated by five water molecules regardless of the water model used. When a softer intramolecular potential is used, however, the TIP3P and TIP5P models exhibit coordination numbers greater than five, as can be seen in the NI plots in Fig. 5 and also in Table 6. A coordination number of 5.4 is observed for the TIP3P model, while the TIP5P model gives a higher coordination number of 6.4. This suggests that bond and angle flexibility serves to enhance the coordination of water around UO_2^{2+}. Because it is known experimentally that there are five waters of hydration surrounding UO_2^{2+}, the TIP3P and TIP5P water models are not recommended for use with the intramolecular parameters recommended here.

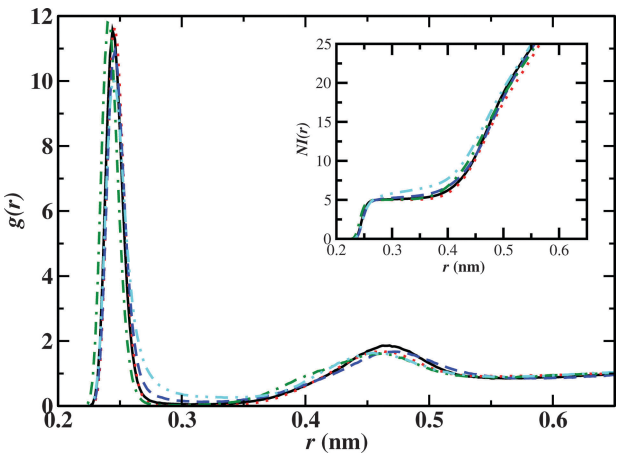

Fig. 5 RDFs and number integrals (inset) for U$\cdots$O$_w$ for UO_2^{2+} in different water models. Black, red, blue, green and cyan colors represent SPC/Fw, SPC/E, TIP3P, TIP4P and TIP5P water models, respectively.

Table 6 Hydration free energies (ΔG_{hyd}) of UO_2^{2+} and average number of water molecules in the first solvation shell (N) of UO_2^{2+} for different water models. Subscripts are uncertainity in the last digit

	ΔG_{hyd}[a] (kJ mol^{-1})		
Water model	This work	Rai *et al.*[24]	N
SPC/Fw	−1409	−1432	5.0897_8
SPC/E	−1390	—	5.0254_3
TIP3P	−1416	−1413	5.3540_{110}
TIP4P	−1383	−1384	5.0254_3
TIP5P	−1480	−1477	6.4360_{30}

[a] Error in ΔG_{hyd} are less than 1 kJ mol^{-1}.

Hydration free energies of the hybrid UO_2^{2+} model in the different water models was also computed and compared to previous published work.[24] Results are shown in Table 6. The hydration free energy for the TIP5P and TIP3P water models is similar to that obtained for the other models, despite the fact that these models have more than five waters surrounding the UO_2^{2+} ion. The added flexibility of the ion resulted in a reduction of the computed hydration free energy in the SPC/Fw model by 25 kJ mol^{-1}. Overall it appears that the hydration free energy is not extremely sensitive to the intramolecular parameters of the actinyl ion.

4 Conclusion

A class I force field has been developed that accurately models the interactions of actinyl ions (AnO_2^{n+}, where, An = U, Np, Pu, Am and n = 1, 2) with water. Water was modeled with the extended simple point charge potential (SPC/E). Intramolecular interactions for the actinyl ions were modeled with harmonic functions, with parameters derived by fitting energy differences computed with density functional theory for small perturbations in the bond lengths and bond angles. The effect of solvation on the intramolecular interactions was treated using a combination of explicit and implicit methods. The proposed intramolecular parameters result in a more flexible UO_2^{2+} ion as compared to previously used potentials.[24,32]

Intermolecular interactions between the actinyl ions and water were modeled with a pairwise Lennard-Jones plus Coulomb potential. To develop the parameters, potential energy surfaces (PESs) between water and an explicitly solvated actinyl ion were computed at the MP2 level and then fit to the force field function. The PESs could be adequately fit by using a common set of Lennard-Jones parameters for the actinyl atom and bonded oxygen atoms. Each ion required a unique set of partial charges, however, to match the computed PES.

The new force field was then used to carry out condensed phase molecular dynamics simulations of each ion in water. Computed An$\equiv$O and An$\cdots$O$_w$ bond lengths were found to be in good agreement with both experiment and previous computational studies. Water coordination numbers also matched known experimental values. Hydration free energies were

computed and compared against literature values and results obtained from quantum calculations in which a solvation model was used. Within the rather large uncertainties involved in all the methods, and given the different assumptions involved in each calculation, the results were generally consistent.

The sensitivity of computed results to the type of water model used was tested by carrying out additional molecular dynamics simulations on UO_2^{2+} in four other water models (SPC/Fw, TIP3P, TIP4P, and TIP5P) using the intramolecular potential developed here but an intermolecular potential developed in earlier work.[24] When a softer intramolecular potential function is used, it was found that the TIP3P and TIP5P models exhibit coordination numbers greater than the known value of five, suggesting that they overbind water. Hydration free energies were less sensitive to the type of potential, however, suggesting that this is not a particularly useful measure to validate force fields.

Acknowledgements

Work of VP and WFS was supported by the Los Alamos Laboratory Directed Research and Development Program. SPT and NR were supported by Materials Science of Actinides, an Energy Frontier Research Center funded by the U.S. Department of Energy, Office of Science, Office of Basic Energy Sciences under award number DE-SC0001089. EJM was supported jointly by both funding agencies. Computational resources were provided by University of Notre Dame Center for Research Computing and the National Energy Research Scientific Computing Center (NERSC). Computational resources on NERSC was supported by the Office of Science, U.S. Department of Energy under contract number DE-AC02-05CH11231.

References

1 R. G. Denning, *J. Phys. Chem. A*, 2007, **111**, 4125–4143.
2 G. Choppin, *J. Radioanal. Nucl. Chem.*, 2007, **273**, 695–703.
3 R. Guillaumont and F. Mompean, *Update on the Chemical Thermodynamics of Uranium, Neptunium, Plutonium, Americium and Technetium*, Elsevier, Amsterdam, 2003.
4 L. R. Morss, N. M. Edelstein, J. Fuger and J. J. Katz, *The Chemistry of the Actinide and Transactinide Elements*, Springer, 2006.
5 K. E. Knope and L. Soderholm, *Chem. Rev.*, 2013, **113**, 944–994.
6 J. K. Gibson, R. G. Haire, M. Santos, J. Marçalo and A. Pires de Matos, *J. Phys. Chem. A*, 2005, **109**, 2768–2781.
7 Y. Marcus, *J. Inorg. Nucl. Chem.*, 1975, **37**, 493–501.
8 Y. Marcus, *Ion Solvation*, John Wiley and Sons Ltd, 1985, pp. 107–125.
9 Y. Marcus and A. Loewenschuss, *J. Chem. Soc., Faraday Trans. 1*, 1986, **82**, 2873–2886.
10 Y. Marcus, *Ion properties*, CRC Press, 1997.
11 J. R. Brand and J. W. Cobble, *Inorg. Chem.*, 1970, **9**, 912–917.
12 S. Tsushima, U. Wahlgren and I. Grenthe, *J. Phys. Chem. A*, 2006, **110**, 9175–9182.
13 L. H. Jones and R. A. Penneman, *J. Chem. Phys.*, 1953, **21**, 542.
14 L. Basile, J. Sullivan, J. Ferraro and P. LaBonville, *Appl. Spectrosc.*, 1974, **28**, 142–145.
15 L. M. Toth and G. M. Begun, *J. Phys. Chem.*, 1981, **85**, 547–549.
16 C. Madic, G. Begun, D. Hobart and R. Hahn, *Inorg. Chem.*, 1984, **23**, 1914–1921.
17 I. Grenthe, J. Fuger, R. Konings, R. Lemire, A. Muller, C. Nguyen-Trung, H. Wanner and I. Forest, *Chemical Thermodynamics of Uranium*, Nuclear Energy Agency, 2004.
18 R. Silva, G. Bidoglio, M. Rand, P. Robouch, H. Wanner and I. Puigdomenech, *Chemical Thermodynamics of Americium*, Elsevier, New York, 1995.
19 H. H. Cornehl, C. Heinemann, J. Maralo, A. P. de Matos and H. Schwarz, *Angew. Chem., Int. Ed. Engl.*, 1996, **35**, 891–894.
20 W. Hummel, G. Anderegg, L. Rao, I. Puigdomenech and O. Tochiyama, *Chemical Thermodynamics of Compounds and Complexes of U, Np, Pu, Am, Tc, Se, Ni, and Zr with Selected Organic Ligands. Chemical Thermodynamics Vol. 9*, Elsevier, Amsterdam, 2005.
21 M. Bühl and G. Wipff, *ChemPhysChem*, 2011, **12**, 3095–3105.
22 H. J. C. Berendsen, J. R. Grigera and T. P. Straatsma, *J. Phys. Chem.*, 1987, **91**, 6269–6271.
23 Y. Wu, H. L. Tepper and G. A. Voth, *J. Chem. Phys.*, 2006, **124**, 24503.
24 N. Rai, S. P. Tiwari and E. J. Maginn, *J. Phys. Chem. B*, 2012, **116**, 10885–10897.
25 D. Hagberg, E. Bednarz, N. M. Edeistein and L. Gagliardi, *J. Am. Chem. Soc.*, 2007, **129**, 14136–14137.
26 F. Réal, M. Trumm, V. Vallet, B. Schimmelpfennig, M. Masella and J.-P. Flament, *J. Phys. Chem. B*, 2010, **114**, 15913–15924.
27 C. Beuchat, D. Hagberg, R. Spezia and L. Gagliardi, *J. Phys. Chem. B*, 2010, **114**, 15590–15597.
28 R. Atta-Fynn, E. J. Bylaska, G. K. Schenter and W. A. de Jong, *J. Phys. Chem. A*, 2011, **115**, 4665–4677.
29 W. L. Jorgensen, J. Chandrasekhar, J. D. Madura, R. W. Impey and M. L. Klein, *J. Chem. Phys.*, 1983, **79**, 926.
30 M. W. Mahoney and W. L. Jorgensen, *J. Chem. Phys.*, 2000, **112**, 8910–8922.
31 P. Guilbaud and G. Wipff, *J. Phys. Chem.*, 1993, **97**, 5685–5692.
32 P. Guilbaud and G. Wipff, *THEOCHEM*, 1996, **366**, 55–63.
33 M. Druchok, T. Bryk and M. Holovko, *J. Mol. Liq.*, 2005, **120**, 11–14.
34 M. J. Frisch, G. W. Trucks, H. B. Schlegel, G. E. Scuseria, M. A. Robb, J. R. Cheeseman, G. Scalmani, V. Barone, B. Mennucci, G. A. Petersson, H. Nakatsuji, M. Caricato, X. Li, H. P. Hratchian, A. F. Izmaylov, J. Bloino, G. Zheng, J. L. Sonnenberg, M. Hada, M. Ehara, K. Toyota, R. Fukuda, J. Hasegawa, M. Ishida, T. Nakajima, Y. Honda, O. Kitao, H. Nakai, T. Vreven, J. A. Montgomery Jr, J. E. Peralta, F. Ogliaro, M. Bearpark, J. J. Heyd, E. Brothers, K. N. Kudin, V. N. Staroverov, R. Kobayashi, J. Normand, K. Raghavachari, A. Rendell, J. C. Burant, S. S. Iyengar,

J. Tomasi, M. Cossi, N. Rega, J. M. Millam, M. Klene, J. E. Knox, J. B. Cross, V. Bakken, C. Adamo, J. Jaramillo, R. Gomperts, R. E. Stratmann, O. Yazyev, A. J. Austin, R. Cammi, C. Pomelli, J. W. Ochterski, R. L. Martin, K. Morokuma, V. G. Zakrzewski, G. A. Voth, P. Salvador, J. J. Dannenberg, S. Dapprich, A. D. Daniels, O. Farkas, J. B. Foresman, J. V. Ortiz, J. Cioslowski and D. J. Fox, Gaussian 09, Revision B.1.

35 W. Küchle, M. Dolg, H. Stoll and H. Preuss, *J. Chem. Phys.*, 1994, **100**, 7535–7542.

36 X. Cao, M. Dolg and H. Stoll, *J. Chem. Phys.*, 2003, **118**, 487–496.

37 X. Cao and M. Dolg, *THEOCHEM*, 2004, **673**, 203–209.

38 J. T. H. Dunning, *J. Chem. Phys.*, 1989, **90**, 1007–1023.

39 K. A. Peterson and T. H. Dunning, *J. Chem. Phys.*, 2002, **117**, 10548–10560.

40 D. Feller, *J. Comput. Chem.*, 1996, **17**, 1571–1586.

41 K. L. Schuchardt, B. T. Didier, T. Elsethagen, L. Sun, V. Gurumoorthi, J. Chase, J. Li and T. L. Windus, *J. Chem. Inf. Model.*, 2007, **47**, 1045–1052.

42 *Energy-Consistent Pseudopotentials of the Stuttgart/Cologne Group*, http://www.theochem.uni-stuttgart.de/pseudopotentials/clickpse.html, Accessed: 2013-04-10.

43 C. Lee, W. Yang and R. G. Parr, *Phys. Rev. B: Condens. Matter Mater. Phys.*, 1988, **37**, 785–789.

44 A. D. Becke, *J. Chem. Phys.*, 1993, **98**, 5648–5652.

45 P. J. Stephens, F. J. Devlin, C. F. Chabalowski and M. J. Frisch, *J. Phys. Chem.*, 1994, **98**, 11623–11627.

46 C. Møller and M. S. Plesset, *Phys. Rev.*, 1934, **46**, 618–622.

47 G. Scalmani and M. J. Frisch, *J. Chem. Phys.*, 2010, **132**, 114110.

48 S. F. Boys and F. Bernardi, *Mol. Phys.*, 1970, **19**, 553–566.

49 S. Spencer, L. Gagliardi, N. C. Handy, A. G. Ioannou, C.-K. Skylaris, A. Willetts and A. M. Simper, *J. Phys. Chem. A*, 1999, **103**, 1831–1837.

50 M. S. K. Fuchs, A. M. Shor and N. Rösch, *Int. J. Quantum Chem.*, 2002, **86**, 487–501.

51 L. V. Moskaleva, S. Krüger, A. Spörl and N. Rösch, *Inorg. Chem.*, 2004, **43**, 4080–4090.

52 P. J. Hay, R. L. Martin and G. Schreckenbach, *J. Phys. Chem. A*, 2000, **104**, 6259–6270.

53 C. P. Kelly, C. J. Cramer and D. G. Truhlar, *J. Phys. Chem. B*, 2006, **110**, 16066–16081.

54 V. S. Bryantsev, M. S. Diallo and W. A. Goddard III, *J. Phys. Chem. B*, 2008, **112**, 9709–9719.

55 J. A. Keith and E. A. Carter, *J. Chem. Theory Comput.*, 2012, **8**, 3187–3206.

56 Z. Cao and K. Balasubramanian, *J. Chem. Phys.*, 2005, **123**, 114309.

57 G. A. Shamov and G. Schreckenbach, *J. Phys. Chem. A*, 2005, **109**, 10961–10974.

58 G. A. Shamov and G. Schreckenbach, *J. Phys. Chem. A*, 2006, **110**, 12072.

59 K. E. Gutowski and D. A. Dixon, *J. Phys. Chem. A*, 2006, **110**, 8840–8856.

60 G. Schreckenbach, P. J. Hay and R. L. Martin, *Inorg. Chem.*, 1998, **37**, 4442–4451.

61 S. Tsushima, T. Yang and A. Suzuki, *Chem. Phys. Lett.*, 2001, **334**, 365–373.

62 S. Tsushima and T. Reich, *Chem. Phys. Lett.*, 2001, **347**, 127–132.

63 W. A. de Jong, R. J. Harrison, J. A. Nichols and D. A. Dixon, *Theor. Chem. Acc.*, 2001, **107**, 22–26.

64 Z. Cao and K. Balasubramanian, *J. Chem. Phys.*, 2009, **131**, 164504.

65 N. G. Tsierkezos, J. Roithová, D. Schröder, M. Ončák and P. Slavíček, *Inorg. Chem.*, 2009, **48**, 6287–6296.

66 G. Schreckenbach and G. A. Shamov, *Acc. Chem. Res.*, 2009, **43**, 19–29.

67 D. Rios, M. C. Michelini, A. F. Lucena, J. Marçalo, T. H. Bray and J. K. Gibson, *Inorg. Chem.*, 2012, **51**, 6603–6614.

68 R. L. Martin, P. J. Hay and L. R. Pratt, *J. Phys. Chem. A*, 1998, **102**, 3565–3573.

69 B. Hess, C. Kutzner, D. van der Spoel and E. Lindahl, *J. Chem. Theory Comput.*, 2008, **4**, 435–447.

70 D. Van Der Spoel, E. Lindahl, B. Hess, G. Groenhof, A. E. Mark and H. J. C. Berendsen, *J. Comput. Chem.*, 2005, **26**, 1701–1718.

71 T. Darden, D. York and L. Pedersen, *J. Chem. Phys.*, 1993, **98**, 10089–10092.

72 U. Essmann, L. Perera, M. L. Berkowitz, T. Darden, H. Lee and L. G. Pedersen, *J. Chem. Phys.*, 1995, **103**, 8577–8593.

73 S. Miyamoto and P. A. Kollman, *J. Comput. Chem.*, 1992, **13**, 952–962.

74 W. G. Hoover, *Phys. Rev. A*, 1985, **31**, 1695–1697.

75 C. H. Bennett, *J. Comput. Phys.*, 1976, **22**, 245–268.

76 V. Vallet, U. Wahlgren, B. Schimmelpfennig, H. Moll, Z. Szabó and I. Grenthe, *Inorg. Chem.*, 2001, **40**, 3516–3525.

77 H. A. Thompson, G. E. Brown Jr and G. A. Parks, *Am. Mineral.*, 1997, **82**, 483–496.

78 P. Allen, J. Bucher, D. Shuh, N. Edelstein and T. Reich, *Inorg. Chem.*, 1997, **36**, 4676–4683.

79 U. Wahlgren, H. Moll, I. Grenthe, B. Schimmelpfennig, L. Maron, V. Vallet and O. Gropen, *J. Phys. Chem. A*, 1999, **103**, 8257–8264.

80 T. Reich, G. Bernhard, G. Geipel, H. Funke, C. Hennig, A. Rossberg, W. Matz, N. Schell and H. Nitsche, *Radiochim. Acta*, 2000, **88**, 633.

81 A. L. Ankudinov, S. D. Conradson, J. Mustre de Leon and J. J. Rehr, *Phys. Rev. B: Condens. Matter Mater. Phys.*, 1998, **57**, 7518–7525.

82 S. D. Conradson, *Appl. Spectrosc.*, 1998, **52**, 252A–279A.

83 M. Di Giandomenico, C. L. Naour, E. Simoni, D. Guillaumont, P. Moisy, C. Hennig, S. D. Conradson and C. Den Auwer, *Radiochim. Acta*, 2009, **97**, 347–353.

84 A. Ikeda-Ohno, C. Hennig, A. Rossberg, H. Funke, A. C. Scheinost, G. Bernhard and T. Yaita, *Inorg. Chem.*, 2008, **47**, 8294–8305.

85 J. M. Combes, C. J. Chisholm-Brause, G. E. Brown Jr, G. A. Parks, S. D. Conradson, P. G. Eller, I. R. Triay, D. E. Hobart and A. Miejer, *Environ. Sci. Technol.*, 1992, **26**, 376–382.

86 K. Takao, S. Takao, A. C. Scheinost, G. Bernhard and C. Hennig, *Inorg. Chem.*, 2009, **48**, 8803–8810.
87 G. Choppin and L. Rao, *Radiochim. Acta*, 1984, **37**, 143–146.
88 G. Choppin, *Radiochim. Acta*, 1983, **32**, 43–53.
89 N. Kaltsoyannis, P. J. Hay, J. Li, J.-P. Blaudeau and B. E. Bursten, *The Chemistry of the Actinide and Transactinide Elements*, Springer, 2006, pp. 1893–2012.
90 D. Hagberg, G. Karlstrom, B. O. Roos and L. Gagliardi, *J. Am. Chem. Soc.*, 2005, **127**, 14250–14256.
91 E. Mauerhofer, K. P. Zhernosekov and F. Rösch, *Radiochim. Acta*, 2004, **92**, 5–10.
92 R. Antonio, L. Soderholm, C. W. Williams, J.-P. Blaudeau and B. E. Bursten, *Radiochim. Acta*, 2001, **89**, 17.